Author Manuscript

Authors: Hannah M.C. Lant; Thoe K. Michaelos; Liam S. Sharninghausen; Brandon Q. Mercado; Robert H. Crabtree; Gary Brudvig

N,N,O Pincer Ligand with a Deprotonatable Site that Promotes Redox-Leveling, High Mn Oxidation States, and a Mn$_2$O$_2$ Dimer Competent for Catalytic Oxygen Evolution

Hannah M.C. Lant[a][‡], Thoe K. Michaelos[b][‡], Liam S. Sharninghausen[c]; Brandon Q. Mercado[a]; Robert H. Crabtree[a]*, Gary W. Brudvig[a]*

[a]   Ms. Hannah Lant, Dr. Brandon Mercado, Dr. Robert Crabtree, and Dr. Gary Brudvig
       Department of Chemistry, Yale University
       225 Prospect St, New Haven CT 06511
[b]   Dr. Thoe Michealos
       Current Address: Components Research Group, Intel Corp,
       2501 NE Century Blvd, M/S RA3-252, Hillsboro, OR 97124
[c]   Dr. Liam Sharninghausen
        Current Address: Department of Chemistry, University of Michigan
   930 North University Ave, Ann Arbor, MI 48109
[‡]   Equal contribution
       *gary.brudvig@yale.edu
       https://brudviglab.yale.edu/
       *robert.crabtree@yale.edu
       https://chem.yale.edu/people/robert-crabtree

       Supporting information for this article is given via a link at the end of the document

Abstract: The new complex [Mn(bipyalk)(H$_2$O)(μ-O)$_2$Mn(bipyalk)](OTf)$_2$ (bipyalk = 2-([2,2'-bipyridin]-6-yl)propan-2-ate) catalyzes oxygen evolution with a TOF of 0.0055 s^{-1} when driven by the sacrificial oxidant KHSO$_5$ in water. It is proposed on the basis of EPR experiments that the catalyst proceeds through a Mn^V(μ-O)$_2$Mn^V=O intermediate supported by the highly donating tertiary alkoxide moiety of the ligand. The Mn(IV,IV) dimer can also be formed electrochemically from its precursor, Mn(bipyalkH)Cl$_2$. A related series of bis-ligated monomers of the type [Mn^n(bipyalkH$_x$)(bipyalkH$_y$)](PF$_6$)$_2$ is also reported, where the dication features Mn^{II}, Mn^{III}, and Mn^{IV} oxidation states and corresponding protonation states. Electrochemical data on this series underscore the importance of proton loss at the alcohol/alkoxide moiety during oxidation to maintain low overpotentials required for catalysis.

Introduction

Artificial photosynthetic systems aim to produce chemical fuels by mimicking natural photosynthesis, which generates reducing equivalents needed for the synthesis of sugars through the sunlight-driven water-splitting reaction (eq 1).[1]

$$2 \ H_2O \rightarrow 4 \ H^+ + 4 \ e^- + O_2 \qquad E° = 1.23 \ V \qquad (1)$$
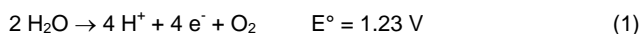
In green plants and cyanobacteria, this reaction occurs at the tetramanganese oxygen-evolving complex (OEC) in Photosystem II (PSII). This oxomanganese cluster stores four oxidizing equivalents during enzyme turnover, cycling through oxidation states that range from Mn$^{III}_3$Mn^{IV} at the most reduced state to Mn$^{IV}_4$-O• or Mn$_3^{IV}$Mn^V=O as the most oxidized state in which O–O bond formation is triggered.[2],[3],[4] Some of the most active artificial water-oxidation catalysts to date are rare and expensive second- and third-row transition metals like Ru and Ir.[5][6], However, as manganese is the third-most abundant transition metal in the Earth's crust,[7] it represents an important target for the sustainable development of synthetic water-oxidation catalysts (WOCs). In addition, biomimetic Mn catalysts may provide information to guide research on the OEC. In turn, we can utilize design principles gleaned from an understanding of the function of the OEC for the development of Mn WOCs.

Despite increased attention on first-row transition metals for water-oxidation catalysis and extensive effort in generating biomimetic manganese complexes, relatively few molecular Mn-based WOCs are known. In 1999,[8] our groups found that [Mn^{III}(terpy)(H$_2$O)(μ-O)$_2$Mn^{IV}(terpy)(H$_2$O)](NO$_3$)$_3$, (terpy = 2,2':6',2"-terpyridine), evolves oxygen when driven by the chemical oxidants NaOCl or KHSO$_5$, the latter giving a TOF of 0.034 s^{-1}.[9] The Mn terpy dimer remains one of the most active Mn-based oxygen-evolution catalysts known, but like many other Mn catalysts in this field[5] it depends on the use of terminal O-donating oxidants to form a high-valent oxo intermediate before reacting with water.[10] Another major limitation has been the longevity of the catalyst, which cycles through both the Mn^{III}(μ-O)$_2$Mn^{IV} and the unobserved O–O bond-forming Mn^{IV}(μ-O)$_2$Mn^V states, the latter of which is reduced by four electrons to the Mn^{II}(μ-O)$_2$Mn^{III} state as water is incorporated

1

with the release of the product oxygen. In this low valent state, protonation of bridging oxo groups likely contributes to catalyst dissociation and degradation. Indeed, dissociation of ligands in the Mn(II) state is a major pathway for decomposition of aqueous Mn complexes in general; avoiding formation of low-valent states is, therefore, seen as central to the further development of robust Mn-based WOCs.

The bulk of homogenous Mn catalysts for oxygen evolution found in the literature are dinuclear complexes like the Mn-terpy dimer described above. The major benefit of multinuclearity is the sharing of charge and accumulation of redox equivalents between metal centers, a concept that extends to many bioinorganic systems such as the OEC.[11][12] Multinuclearity may be part of the design of a catalyst where ligand scaffolds enforce polynuclearity, such as in the work of Åkermark and coworkers.[13],[14] However, in many cases, Mn complexes which begin as monomeric units are observed to dimerize to form active catalysts; an example comes from the work of McKenzie and co-workers, where mononuclear Mn complexes with monoanionic carboxylate-containing pentadentate ligands evolve oxygen when driven by tBuOOH,[15] and are thought to dimerize during turnover via a bridging carboxylate group from the ligand scaffold. Despite the benefits of having multiple metal sites, multi-nuclear Mn complexes are not guaranteed to be active catalysts; as an example, Agapie and coworkers were able to make tri- and tetra-nuclear clusters with remarkable geometric resemblance to the OEC, but none showed oxygen-evolving activity.[16][17][18]

Another approach to enhance activity is to incorporate anionic donors into ligand scaffolds, which can facilitate attainment of higher oxidation states and avoid degradation, and this has been a theme in the development of Mn-based synthetic WOCs. A previous study from our group that utilized pentadentate ligands to generate mononuclear Mn catalysts saw that, in addition to the number of negative donor groups, their location relative to open site for substrate binding was critical to modulating reactivity. By placing a negative charge *trans* to a substrate binding site, these ligands may not only enhance the catalytic rate by destabilizing the key oxo intermediate, but may also favor the less labile Mn^{III} state over the Mn^{II} state that would otherwise be formed.[19] Anionic ligands or basic groups have been used to assist in shuttling protons either to or away from active sites in various oxidation[20],[21] or reduction[22],[23] reactions, mimicking design principles from bioinorganic reaction sites, for example, the proton relays of the OEC.[24],[25]

A key goal in the field is to generate electrochemically active catalysts for use in artificial photosynthetic systems. Few examples of homogenous Mn-based water-oxidation electrocatalysts have been reported, the earliest being a Mn porphyrin dimer with a reported TOF of 0.11 min^{-1}.[26] Examples from 2014 include a dimanaganese complex[27] ligated by a Schiff-base macrocyle which gives 11 turnovers at 1.3V vs. $Fc^{+/0}$, and a monomeric $[(Py_2NtBu_2)Mn(H_2O)_2]^{2+}$ complex which gives about 20 turnovers at pH 12.2 and 800 mV overpotential.[28] The leading example, a recent result from Maayan and coworkers, is a Mn_{12} cluster comprised of Mn^{III}-$(\mu$-O$)_2$-Mn^{IV} units and capped by eight 3,5-dihydroxybenzoate hydrophilic ligands. This cluster exhibits sustained oxygen evolution when driven at the low overpotential of 334 mV at pH 6.[29] While further work on this system may elucidate how a potentially redox non-innocent ligand scaffold can assist manganese centers in catalytic electrochemical oxidation of water, it is likely that both the higher nuclearity and the bulk of the ligand circumvent the production of labile Mn^{II} during catalytic turnover and allow for more robust catalysis.[30]

Among the key functional aspects of the OEC are its ability to support the high oxidation states needed for the formation of the O–O bond, its use of multiple Mn centers, and its avoidance of the labile Mn(II) state. These benefits can be promoted in synthetic catalysts by the incorporation of highly donating anionic oxygen-donor ligands such as oxos or alkoxides. Successfully circumventing the labile[7] high-spin d^5 Mn(II) state should increase the longevity of the catalyst, as the ligand scaffold will be retained when cycling through less labile higher oxidation states. Additionally, incorporation of anionic groups in the ligand scaffold that are able to facilitate the release of protons during turnover may lower the overpotentials needed to drive water oxidation, resembling proton management and redox leveling in the OEC. With these bio-inspired principles in mind, we report a new di-μ-oxo dimanganese complex of the pincer 2-([2,2'-bipyridin]-6-yl)propan-2-ol (bipyalkH), which acts as a strong π-donor upon deprotonation of the alcohol. This ligand incorporates the pyridine alkoxide "pyalk" motif that we previously showed can stabilize high oxidation states in Rh[31] and Ir[32–34] and promote water-oxidation catalysis, both with chemical oxidants and electrochemically, with Ir[35–37] and Cu.[38] We also have previously reported oxygen evolution from our low-valent precatalyst Mn(bipyalkH)Cl$_2$ (**1**, shown in Figure 1) driven by KHSO$_5$ with retention of activity for >160 hrs in unbuffered solutions. In that study, we proposed that a dimeric species formed *in situ* was responsible for catalytic activity.[39] Here we report the synthesis, catalytic activity, and redox behavior of the dimeric species [Mn(bipyalk)(H$_2$O)(μ-O)$_2$Mn(bipyalk)](OTf)$_2$ (**2**). We also demonstrate that **2** can be generated electrochemically.

1: Mn(bipyalkH)Cl$_2$

2: [Mn(bipyalk)(H$_2$O)(μ-O)]$_2$(OTf)$_2$

3: [Mn(bipyalk)(bipyalkH)](PF$_6$)$_2$
x = 0, y= 1, n = 3
4: [Mn(bipyalk)$_2$](PF$_6$)$_2$
x = 0, y= 0, n = 4
5: [Mn(bipyalkH)$_2$](PF$_6$)$_2$
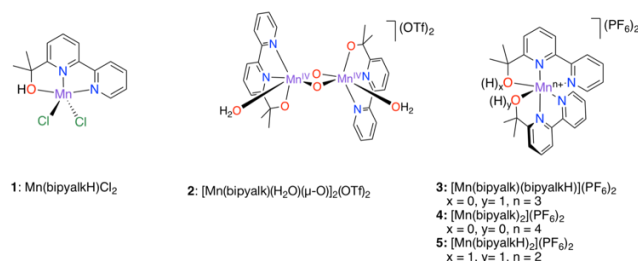x = 1, y= 1, n = 2

Figure 1. Structures of compounds **1-5**.

Results and Discussion

2

Synthesis and Characterization. In our previous work,[39] we proposed that catalytic oxygen evolution from a mononuclear precursor, Mn(bipyalkH)Cl$_2$, **1**, arose from a dimeric active species formed *in situ*, akin to the well-characterized "terpy dimer" [Mn$^{III,IV}_2$(μ-O)$_2$(terpy)$_2$(H$_2$O)$_2$](NO$_3$)$_3$. We have now prepared and isolated **2**, a dimeric species competent for oxygen evolution, which forms upon treatment of **1** with 1.5 equiv. of KHSO$_5$. The crystal structure of **2**, shown in Figure 2, has several features unique from other known Mn$_2$(μ-O)$_2$ dimers. The nine other examples of dimers of the type [Mn$_2$(μ-O)$_2$(L)$_2$(H$_2$O)$_2$]$^{n+}$ (L = pincer) found in the Cambridge Structural Database (CSD) are all isolated in the (III,IV) oxidation state (SI Table S1) while **2** is isolated in the (IV,IV) oxidation state. This oxidation state assignment follows from the presence of two PF$_6^-$ counteranions and the short metal-ligand bond lengths (d(Mn-O$_{alkoxide}$) = 1.833(3) and 1.873(3) Å), all consistent with deprotonated alkoxide ligands. The Mn-Mn distance of 2.71 Å falls in the expected range for Mn$_2$O$_2$ dimers of both the (III,IV) and (IV,IV) oxidation states.[40] The unusually high-valent state of **2** is attributed to the strongly donating tertiary alkoxides. A unique feature of the crystal structure of **2** is the orientation of the water ligands relative to the Mn$_2$O$_2$ core. All other CSD examples of Mn$_2$(μ-O)$_2$ (SI Table S1) feature an inversion center between the Mn centers, with waters bound *trans* to each other. In contrast, **2** has waters bound in a *cis* fashion, a feature that could be implicated in catalysis during O–O bond formation, as has been shown with iron-based WOCs.[41]
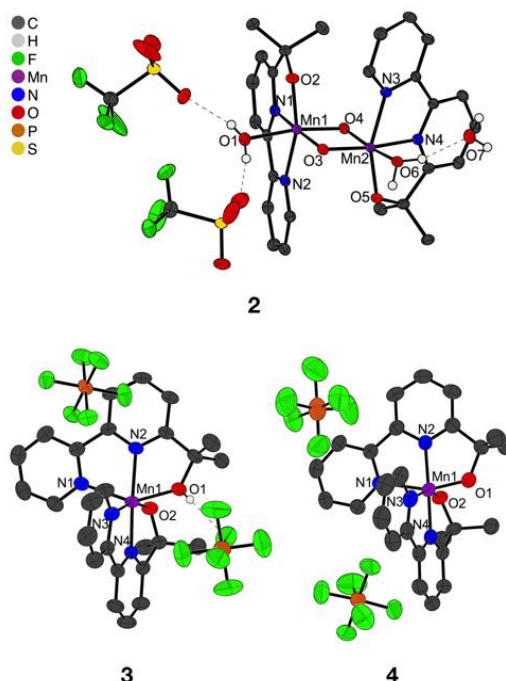

Figure 2. X-ray crystal structures of **2**, **3**, and **4**. For all three structures, thermal ellipsoids are displayed at the 50% probability level and hydrogens except for those bound to heteroatoms are omitted for clarity. For **2**, two triflate counterions and one DCM solvent molecule are omitted for clarity. See Figures S18-S20 for complete scheme and omitted moieties.

The UV-visible spectrum of dimer **2** (Figure S2) has similar features to previously reported Mn di-μ-oxo dimers. Notably, the prominent feature observed at 423 nm has previously been attributed to a d-d transition arising from a Mn(IV) center in Mn(III,IV) and Mn(IV,IV) di-μ-oxo dimers.[42] The intensity of this transition correlates to Mn(IV) content, and the absorbance of **2** at this wavelength is high as is expected for a Mn(IV,IV) species. The peak at 631 nm and the shoulder around 835 nm have both been previously assigned to charge transfer from the bridging oxos to Mn(IV).

We also prepared several novel high-valent coordinatively-saturated Mn monomers with the bipyalk ligand, which have been particularly useful in the spectroelectrochemical characterization of dimer **2**. The Mn(III) and Mn(IV) monomers, **3** and **4**, respectively, were isolated as dications, and their crystal structures are shown in Figure 2. We previously reported[39] the analogous complex in the Mn(II) state, [Mn(II)(bipyalkH)$_2$](PF$_6$)$_2$, (**5**, shown in Figure 1) which is also dicationic. Table 1 contains selected bond angles and distances in this series. Oxidation from Mn(II) to Mn(III) is coupled with a deprotonation at O2 of the ligand scaffold; this is indicated by a 0.39 Å contraction of the Mn1-O2 bond. A similar contraction of the Mn1-O1 bond occurs when O1 is deprotonated upon oxidation from Mn(III) to Mn(IV). Across the series, as oxidation state increases, all bonds angles trend towards the expected 90° for idealized octahedral geometry. This contraction can be rationalized by increased pi bonding from the oxygens upon deprotonation from the alcohol to the alkoxide. The ability to couple deprotonation of the ligand to oxidation of the metal center has a redox-levelling effect on this series, an effect that is expected to extend to the aqueous complexes, including **1** and **2**, and is further discussed with the electrochemical data reported here. This series highlights the importance of the alkoxide functionality of the bipyalk ligand in stabilizing higher oxidation states. While we report the full synthesis and characterization of **3** in this work, attempts to prepare samples of **4**

3

with a high degree of purity have failed. We have chosen to report the crystal structure of **4**, of which the oxidation state is unequivocally indicated on the basis of Mn-O bond lengths indicating anionic functionality, to underscore the importance of this alcohol/alkoxide unit in redox leveling.

	Mn(II)	Mn(III)	Mn(IV)
Mn1-O1	2.224(3)	2.133(2)	1.821(3)
Mn1-O2	2.171(2)	1.8382(17)	1.828(3)
Mn1-N1	2.203(3)	2.203(2)	1.931(3)
Mn1-N2	2.181(3)	2.080(2)	2.083(4)
Mn1-N3	2.229(3)	2.083(2)	2.070(4)
Mn1-N4	2.181(3)	1.957(2)	1.938(4)
O1-Mn1-N2	70.7(1)	73.02(8)	82.15(14)
N1-Mn1-N2	74.31(11)	75.29(8)	78.11(14)
O2-Mn1-N4	70.62(10)	81.75(8)	81.37(13)
O2-Mn1-N4	73.86(11)	77.58(8)	78.39(14)
N3-Mn1-N4	2.224(3)	2.133(2)	1.821(3)

Table 1. X-ray crystallographic bond lengths and angles between Mn center and all atoms in the primary coordination sphere from the series of the bis-ligated monomers **5**, **3**, and **4** which feature oxidation states Mn^{II}, Mn^{III}, Mn^{IV}, as well as two, one, or no protons on the alcohol/alkoxide moiety. Atom labels correspond to those shown in structures in Figure 2, and are consistent with the numbering scheme of **5**, published previously.[39]

Catalysis:

Oxygen Detection and Rate Law. We previously reported that **1** is competent for oxygen evolution and proposed that Mn_2O_2 dimers are responsible for catalysis, in analogy to the well-known terpy dimer system, on the basis of mass spectrometry and UV-visible spectroscopic studies.[39] We were, therefore, intrigued to explore the oxygen-evolution activity of dimer **2**. Indeed, we demonstrate here that isolated **2** is active for oxygen-evolution catalysis, with a typical oxygen-evolution trace shown in Figure S7. Furthermore, catalysis with **2** lacks the induction period previously observed[39] when **1** was injected into a solution of $KHSO_5$, which we ascribed to time needed for the formation of catalytically active multinuclear species. Under typical reaction conditions of 10 mM sacrificial oxidant and 50 µM catalyst, **2** gives a TOF of 0.0055 mol O_2 per mol **2** per second, or 0.0028 s^{-1} when normalized to total Mn content. Complex **2** is somewhat slower than precatalyst **1** (TOF = 0.0099). Accordingly, while **2** catalyzes oxygen evolution, it is likely not the most active component in the mixture formed upon activation of **1** with $KHSO_5$. Thus, a complex speciation profile of Mn(bipyalk) units is likely at play that may depend highly on pH conditions or buffer anion identity or concentration, similar to the results[6] we have found with the "blue solution" formed from the related Cp*Ir(pyalk)Cl precursor for Ir-based WO. We have examined the role of concentration of sacrificial oxidant $KHSO_5$ under pseudo-first-order conditions of oxidant on the initial rate of oxygen evolution by **2**. Logarithmic plots (Figure S8) indicate that oxygen evolution is first-order in $KHSO_5$. This finding may indicate that an oxidation event of the catalyst is rate-limiting, or that perhaps that O-atom transfer from the oxidant is rate-limiting. While this finding ultimately doesn't indicate the origin of oxygen atoms in product oxygen, we draw an analogy to the similar Mn terpy dimer, which has been shown by ^{18}O-labelling studies to incorporate one ^{18}O labelled atom from solvent water and one ^{16}O atom from $KHSO_5$ under moderate excess oxidant conditions.[9] Further studies including isotope labelling experiments may deduce the origin of O atoms in product oxygen.

EPR measurements Indicating Turnover. To examine oxidation states of the complex before and during catalytic turnover, a solution of sacrificial oxidant was added and frozen over a frozen solution of **2** in wet acetonitrile inside an EPR tube. Prior to mixing of the layers, the sample gives a weak EPR signal indicative a small amount of $Mn^{III,IV}_2O_2$, with the rest of the sample presumably composed of the EPR-silent $Mn^{IV}_2O_2$ state. Thawing for 30 sec. and then refreezing this sample yields an increase in the 16-line signal characteristic[43] of a $Mn^{III}Mn^{IV}$ dimer (Figure 3). The detection of a 1-electron reduced species upon treatment with a two-electron oxidant likely results from comproportionation of $Mn_2^{III,III}$ and $Mn_2^{IV,IV}$ states to form a $Mn^{III}(\mu$-O$)_2Mn^{IV}$ species as shown in Figure 4b. We interpret these results to indicate a $Mn^{IV,IV}_2$ (**I**) $\rightarrow$ $Mn^{V,V}_2$ (**III**) $\rightarrow$ $Mn^{III,III}_2$ (**IV**) cycle resulting in O_2 liberation as shown in Figure 4a. The formation of $Mn_2^{V,V}$ in this system is plausible considering the high donicity of the alkoxide functional groups. Each product O_2 may contain one O atom from peroxymonosulfate and one from water in analogy with the terpy dimer system at high [HSO_5^-] conditions, which is also

4

consistent with the reaction being first order in KHSO$_5$. Furthermore, incorporation of water is required to form the Mn$^{III}_2$ state (**IV**), which is implicated in the formation of **V** as evidenced by the 16-line EPR spectrum.
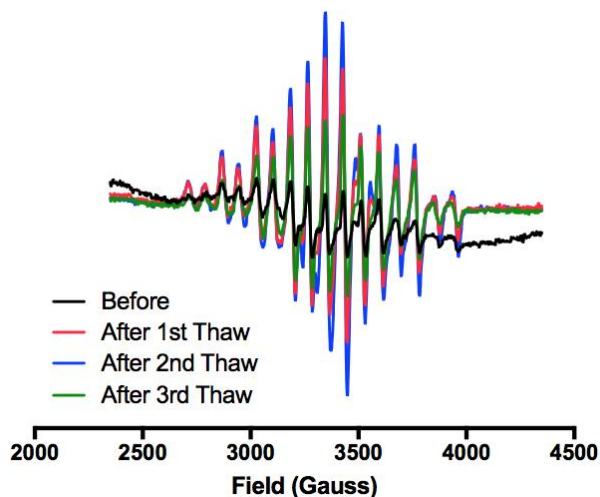

Figure 3. X-band EPR signals recorded after three thaw-freeze cycles. Microwave frequency: 9.37 GHz, microwave power: 0.1 mW, modulation amplitude: 19.49 G. Solution containing **2** at 0.6 mM in wet MeCN with 0.1 M NaTFA to prevent aggregation was frozen and subsequently layered with a solution of 6.0 mM Ph$_4$HSO$_5$ in same NATFA/MeCN mixture.
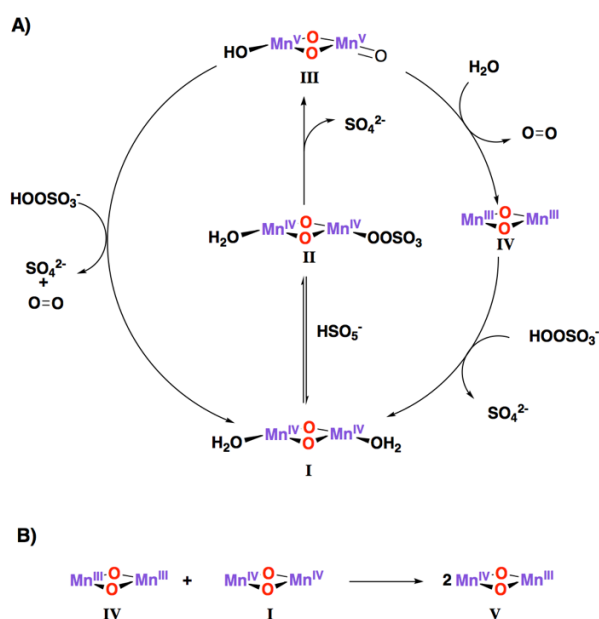

Figure 4. A) Proposed catalytic mechanism based on kinetic and EPR experiments. The left side of the figure represents the proposed mechanism if evolved oxygen arises fully from HSO$_5^-$ incorporation, whereas the right side shows implicated states if water is incorporated. B) Comproportionation reaction scheme proposed to give rise to **V**.

Electrochemistry:
Cyclic Voltammetry and Spectroelectrochemistry of 1 and 2. From both previously published[39] mass spectrometry data and the preparation and isolation of **2** reported here, it is apparent that **2** can be formed from the chemical pre-oxidation of **1**

5

prior to catalysis, though catalytic data above show that **2** may not be the only catalytically active species formed from oxidative treatment of **1**. To further investigate the redox properties of these compounds and evaluate feasibility of electrocatalysis, we turned to cyclic voltammetry. The cyclic voltammagram of **1** (Figure 5a), shows the complex electrochemistry of this system in aqueous solutions; a single large anodic feature is observed at 1.07 V, and two smaller reductive events occur at 0.92 V and 0.46 V. Because assignment of these features was not immediately obvious, we investigated **1** under oxidative conditions using spectroelectrochemistry (SEC).
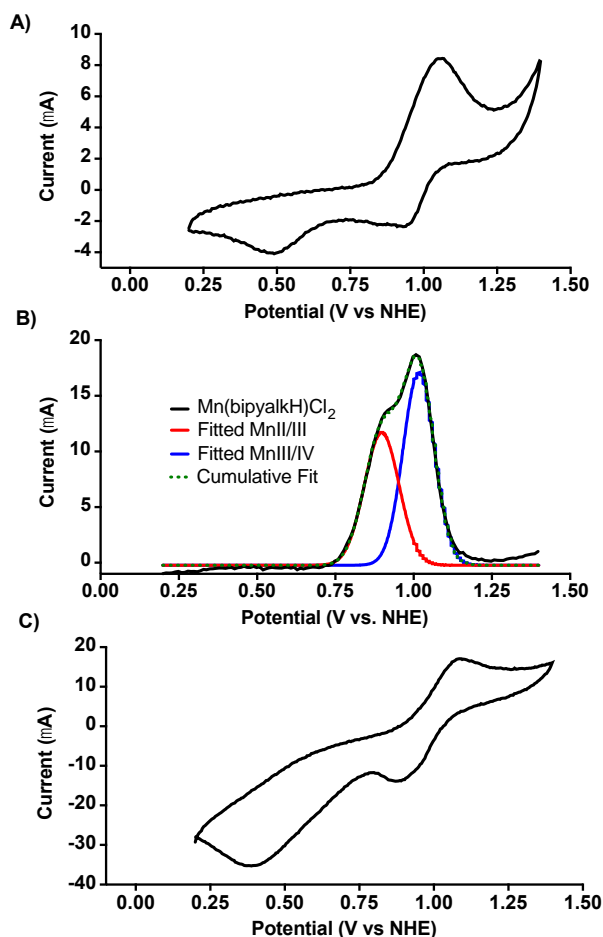

Figure 5. a) CV of **1** (2.5 mM) in 0.1 M acetate buffer at pH 4.47 at 100 mV/s scan rate. Conditions: GC working electrode, Pt wire counter electrode, Ag/AgCl reference electrode. b) Oxidative DPV of **1** under the same conditions with deconvoluted peaks and cumulative fit. c) CV of **2** (1.0 mM) under same conditions as a) and b).

In these SEC experiments, 15-minute oxidizing electrochemical pulses were applied to a solution of **1** in acetate buffer with a spectroelectrochemical Pt electrode that enabled UV-visible spectra to be collected continuously through the duration of these pulses. Each successive pulse applied was 100 mV more oxidizing than the previous. Figure 6a shows the final UV-visible spectrum obtained at each potential. Based on these experiments, **2** or a closely-related dimeric species is formed quantitatively from electrolysis of **1** in acetate buffer at 1.10 V versus NHE at pH = 4.47 as shown in Figure 6a. It appears that the system goes through a Mn(III) species, likely monomeric, at intermediate potentials (800 mV to 1.0 V). A comparison of the spectrum resulting from isolated **3** in acetonitrile and the spectrum found at 900 mV shows that these species are very similar. To further examine this point, we deconvoluted the spectra at each potential and expressed these as a linear combination of the spectra of **1**, **2**, and **3**. From this comparison, it appears that roughly 20% of the Mn content can be accounted for in the form of a Mn(III) monomer at a potential of 900 mV. This may imply that a coordinatively saturated Mn(III) complex with two bipyalk ligands similar to **3** forms at these intermediate potentials, or that only some Mn centers are converted to this oxidation state.
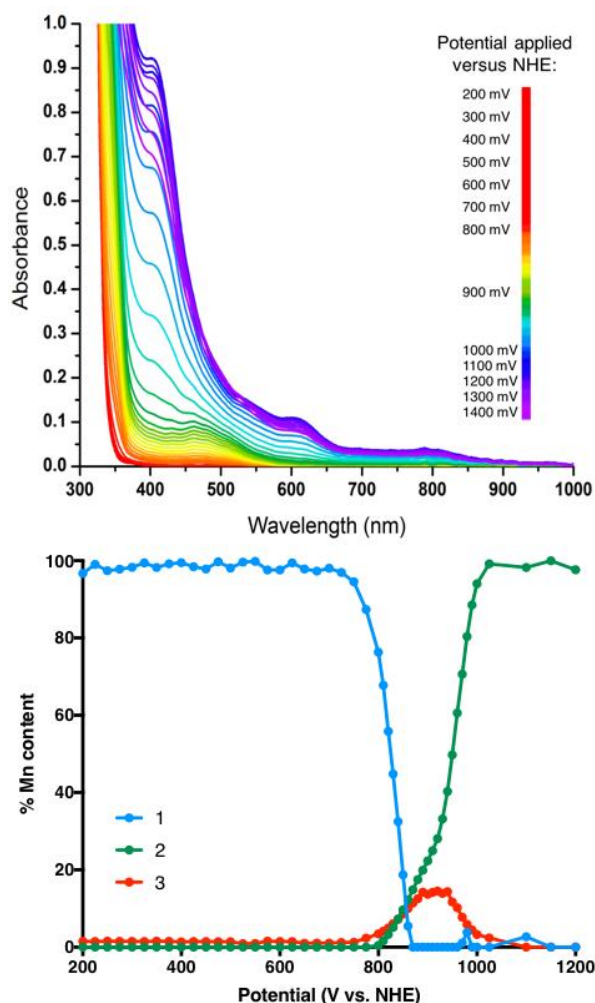
6

Figure 6. a) Series of final UV-Vis spectra obtained at each potential indicated after 15 min of electrolysis to a 2.5 mM solution of 1 in pH 4.47 0.1 M acetate buffer. Conditions: Pt working electrode, Pt wire counter electrode, Ag/AgCl reference electrode. b) Deconvolution of spectra shown in a), modeled as a linear combination of basis UV-vis spectra obtained from **1**, **2**, and **3** recorded at 2.5 mM, 1.25 mM, and 2.5 mM, respectively.

These findings are consistent with bulk electrolysis data. Integration of charge passed during an electrolysis of **1** at 1.2 V versus NHE (Figure S10) indicates a quantitative two-electron oxidation, and UV-visible spectra of these solutions indicate the formation of **2**. Electrolysis at 930 mV yields a spectrum that appears similar to that of **3**, and charge integration shows just under one equivalent of electrons has been passed (Figure S11).

With these findings in mind, we were able to assign the features in the CV of **1**. We attribute the sole anodic feature to two successive oxidative events with very similar $E_{1/2}$'s corresponding to a Mn(II/III) oxidation followed by a Mn(III/IV) oxidation. The i_{pf}/i_{pr} ratio far exceeds unity for this feature, indicating a chemical process following the oxidation which we attribute to *in-situ* dimerization to form **2**. We observe that the E_{pf} for the anodic feature increases with scan rate up to 300 mV s^{-1}. At and above this scan rate, the peak potential remains fixed at 1.07 V vs. NHE. This behavior has been shown to indicate a second-order chemical reaction following an electron transfer, such as dimerization.[44] The reductive processes appear to be more complex, exhibiting cathodic features at 0.92 V and 0.46 V. We assign the first reductive event to the reduction of **2** to its Mn^{III}(μ-O)$_2$Mn^{IV} state; the fact that only one half of the Mn ions would be reduced in this step accounts for the small total current passed in comparison to the oxidative feature. The feature at 0.46 V corresponds to further reduction of the Mn^{III}(μ-O)$_2$Mn^{IV} state to Mn^{III}(μ-O)$_2$Mn^{III}. As the pK_a of bridging oxos between Mn^{III} centers is expected to be more basic relative to those bridging metals at higher oxidation states, protonation of the oxos bridging Mn(III) centers may yield bridging hydroxo groups, favoring dissociation of the dimer. Further reduction of the Mn^{III} monomers to Mn^{II} may then be triggered, which would be more facile in the absence of highly donating oxo ligands. This

7

accounts for the larger relative total current passed for this feature, as a total of ~1.5 reducing equivalents will be passed relative to the total number of Mn centers.

Two anodic features were partially resolved using differential pulse voltammetry (DPV). As shown in Figure 5b, this feature is comprised of an oxidation at 0.90 V which we assign to the Mn(II/III) couple, followed by a Mn(III/IV) couple at 1.02 V. The close spacing of these oxidative features may be attributed to the redox-levelling effect that proton-coupled oxidation of the bipyalk ligand is expected to impart on the redox potentials of these complexes. Deprotonation is expected upon oxidation, as demonstrated by monomers **3** and **4**.

This *in-situ* dimerization is reminiscent of the behavior of similar Mn complexes under oxidizing conditions. The coordinatively-saturated complexes $[Mn(terpy)_2]^{2+}$ and $[Mn(bipy)_2]^{2+}$ are known to form dimers electrochemically once oxidized to the Mn^{IV} state, with the extent of dimerization dependent on both the pH of the solution and the electrolyte.[45] The Mn-terpy dimer is also known to dimerize upon electrochemical oxidation, but does not produce oxygen due to formation of a stable and catalytically inert "dimer of dimers" in the $Mn_4^{IV,IV,IV,IV}$ state.[46],[47]

CVs of **2**, shown in Figure 5c, exhibit similar behavior in comparison to those of **1**, with an anodic feature at 1.10 V and cathodic features at 0.88 V and 0.40 V. The oxidative event with the quasi-reversible return feature at 0.88 V is assigned to the $Mn_2(III,IV/IV,IV)$ couple, and these peak potentials match those of **1**, to within several mVs. However, it appears when the dimer is pre-formed with highly donating oxo bridges, no features indicative of oxidation states lower than $Mn_2^{III,IV}$ are observed on the CV timescale. The cathodic feature at 0.39 V is assigned to reduction to the $Mn_2^{III,III}$ state and then subsequent protonation and dissociation, triggering reduction of the Mn^{III} monomers to Mn^{II} and thus accounting for the large total current passed in this feature.

Evaluation of electrocatalytic activity. Our findings that **2** can be generated *in-situ* electrochemically from **1** prompted us to screen **1** for electrocatalytic water-oxidation activity. As no features in the CV indicated oxygen evolution on the CV-timescale, we investigated **1** for oxygen evolution with a Clark-electrode at 0.5 mM, a ten-fold higher concentration than for Clark-electrode assays with $KHSO_5$. Though conditions under oxidizing potentials ranging from 1.2-1.8 V vs. NHE in acetate buffer with both platinum and glassy carbon working electrodes were examined, no condition was found to produce oxygen over background electrode levels (Figure S13). As has been previously shown,[48] electrode identity and surface pre-treatment often greatly affect redox behavior in facilitating proton-coupled oxidative processes with Mn complexes like those studied here. Future studies may utilize higher surface-area and/or surface-modified electrodes as well as a wider range of pH conditions to check for water oxidation.

Cyclic Voltammetry and Spectroelectrochemistry of 3-5. The importance of proton management is highlighted by the behavior of the organic-soluble bis-ligated monomers **3**-**5**. While we attribute the complex electrochemical behavior of **1** and **2** in aqueous solution to proton-coupled redox events originating from the basic alkoxide functionality of the bipyalk ligand, it appears that lack of proton management in nonaqueous solutions, which are necessary in solvating the series of bis-ligated monomers, precludes the observation of any redox features on the CV timescale (Figure S14). We instead turned to spectroelectrochemistry in order to study the oxidation chemistry of these monomers. For these experiments, the applied potential was successively increased in the oxidative direction every 15 minutes while UV-visible spectra were recorded. Chronoamperograms recorded during each step show that no more oxidative charge is passed by the end of the 15-minute pulse (see Figure S15). As shown in Figure S16, **5** remains in its reduced state until 1.15 V is applied, at which point spectroscopic features indicative of higher oxidation states begin to grow in. These features grow in more rapidly at higher potentials until a UV-visible spectrum of **3** can be overlaid with that produced when 1.45 V is applied to **5**. Electrolysis of complex **3** also shows signs of oxidation (Figure S17), with growing absorbance around 450 nm indicative of formation of Mn^{IV}. No well-defined midpoint potential for this $Mn^{III/IV}$ transition may be assigned, given that the absorbance grows in over a broad range of potentials from 0.55 to 1.45 V, likely owing to the very slow proton-coupled oxidation process occurring under non-aqueous conditions without the presence of a base. Notably, compounds **5** and **3** do not exhibit the same behavior at the same potentials. This is attributed to the fact that deprotonation of the ligand scaffold to allow for subsequent oxidation happens very slowly in nonaqueous media, especially without adding an organic-soluble base; with **5** and **3** being isolated and dissolved at different protonation states, they are able to reach different maximum oxidation states.

Conclusions

We report a novel Mn_2O_2 dimer competent for oxygen evolution when driven by the sacrificial oxidant $KHSO_5$. While functioning similarly to previously reported Mn_2O_2 dimers supported by tridentate ligand scaffolds, the inclusion of the tertiary alkoxide gives rise to several distinct features. First, this highly donating ligand yields a Mn_2O_2 dimer isolable in the Mn^{IV}_2 state, whereas most dimers of this type are isolated in the $Mn^{III,III}_2$ state. We have shown this complex can catalyze oxygen evolution when driven by the sacrificial oxidant $KHSO_5$ with a TOF of 0.0055 s^{-1}. As this TOF is not as fast as the TOF found when an equimolar amount of precursor **1** is pretreated with concentrated $KHSO_5$ prior to catalysis, complex speciation to a variety of Mn-based WOCs is implicated. Further studies will investigate this point under a variety of buffer and pH conditions. Additionally, ^{18}O-labelling experiments will investigate the origin of O atoms in product oxygen as $KHSO_5$ is known as a oxo-transfer reagent. Based on EPR experiments, we propose that this complex passes through an unusually high $Mn^{V,V}_2$ state at the O–O bond-forming step. We also observed the redox-levelling effect imparted by the alcohol/alkoxide group; in addition to observing successive deprotonations with increasing oxidation state in the crystal structures of the monomeric series **5**, **3**, and **4**, the redox-leveling effect was highlighted by the similarity in mid-point potentials of the Mn(II/III) redox couple of **5** and the Mn(III/IV) redox couple of **3** in non-aqueous media, where no added acids or bases are present to aid in shuttling protons, as shown through spectroelectrochemistry experiments.

8

Similar behavior is presumed in the case of **1**, where the CV indicates that Mn (II/III) and Mn(III/IV) couples occur so close together that they could only be resolved via DPV. This behavior is analogous to that which occurs at the OEC in natural photosynthesis, where proton-coupled electron transfer (PCET) steps release protons from substrate waters upon oxidation in order to mitigate energy barriers associated with successive oxidations. While **2** does not function as an electrocatalyst for water oxidation, use of the bipyalkH scaffold for low overpotentials imparted by this redox leveling effect is a promising approach for use with higher nuclearity Mn clusters or other transition metals in the development of electrocatalysts for water oxidation, as well as the observation of high oxidation states.

Experimental

Syntheses:
Preparation of [Mn^{IV}$_2$(μ-O)$_2$(bipyalk)$_2$(H$_2$O)$_2$](OTf)$_2$ (2). A pale yellow stirred solution of Mn(bipyalkH)Cl$_2$ (prepared according to published methods,[39] 0.35 mmol, 119.6 mg) in Milli-Q water (10 mL) was cooled to 0 °C. The dropwise addition of solution of Oxone (0.525 mmol, 1.5 equiv) in Milli-Q water (5 mL) at 0 °C caused a color change to a deep olive-brown. The reaction was allowed to proceed for 20 mins in an ice bath, and then an additional 10 mins at room temperature. For isolation, several drops (0.1 mL) of a saturated solution of NaOTf in Milli-Q water were added. The solution was subsequently extracted with DCM to remove red high-valent coordinatively saturated monomers. The resulting aqueous solution was reduced in volume by two-thirds with a stream of compressed air, and refrigeration overnight yielded a precipitate of dark olive-green crystalline material suitable for X-ray diffraction. This material was filtered and rinsed with DCM and water at 0 °C. Yield: 62.9 mg (40.0%). UV-visible spectrum (MeCN) λ_{max} (ε) = 241.9 (26,495), 296.1 (19970), 423.1 (2976), 500.9 (1115), 630.9 (468), 835.9 nm (136.7 mol dm^3 cm^{-1}). IR (solid): υ = 406.9, 427.7, 555.1, 638.5, 646.2, 664.8, 727.4, 740.5, 777.5, 833.8, 963.4, 1022.7, 1043.8, 1097.7, 1131.1, 1201.7, 1259.1, 1301.7, 1366.9, 1452.6, 1495.7, 1578.2, 1603.3, 2011.1 cm^{-1}.

Preparation of [Mn^{III}(bipyalkH)(bipyalk)(PF$_6$)$_2$] (3). A solution of bipyalkH (81 mg, 0.38 mmol) in acetone (2 mL) was added dropwise to a stirred solution of Mn(OAc)$_2$•4H$_2$O (44 mg, 0.18 mol) in water (2 mL) to produce a yellow, cloudy solution. A solution of Oxone (0.11 KHSO$_5$, 0.55 equiv.) in water (1 mL) was added dropwise, yielding an orange-red solution. After allowing the mixture to stir for five minutes, several mL of a saturated solution of KPF$_6$ was added. For isolation, DCM was added (10 mL) to extract a red colored material. This layer was separated and dried over Na$_2$SO$_4$. A red sticky precipitate was formed via dropwise addition of diethyl ether. The supernatant was removed and triturated with diethyl ether until solid was free flowing to remove all excess free bipyalkH ligand. Yield: 82%. Crystals were grown by dissolving the resulting powder in DCM and layering with pentanes. UV-visible spectrum (MeCN) λ_{max} (ε) = 241.9 (26,495), 296.1 (19,970), 423.1 (2,976), 500.9 (1,115). 630.9 (468), 835.9 nm (136.7 mol dm^3 cm^{-1}). IR (solid): υ = 406.9, 427.7, 555.1, 638.5, 646.2, 664.8, 727.4, 740.5, 740.5, 777.5, 833.8, 963.4, 1022.7, 1043.8, 1097.7, 1131.1, 1201.7, 1259.1, 1301.7, 1366.9, 1452.6, 1578.2, 1578.2, 1603.3, 2011.0 cm^{-1}.

Preparation of [Mn^{IV}(bipyalk)$_2$](PF$_6$)$_2$ (4). Crystals of **4** were obtained from a preparation of an analogous preparation of **2** with KPF$_6$. Crystals suitable for diffraction were found after several weeks. Attempts to directly synthesize **4** via preparations analogous to that of **3** with excess Oxone gave mixtures of **3** and **4** on the basis of UV-visible spectra.

Mass Spectrometry:
Bulk purity was assessed using high-resolution mass spectrometry. The mass spectral data were obtained from a Thermo Scientific (Waltham, MA) LTQ Orbitrap Fusion mass spectrometer. The sample was directly infused into the mass spectrometry via a micro pump. Data were acquired and analyzed with Xcalibur (v2.1; Resolution, 120,000; mass range (m/z) 100 - 700). Exact masses were obtained for the entire broadband spectrum.

Spectroscopy:
UV-visible spectra were recorded on a Cary 50 spectrophotometer. Attenuated total reflectance Fourier transform infrared (ATR-FTIR) spectra were recorded with a PIKE technologies GladiATR.

Oxygen-Evolution Quantification with Clark Electrode:
A Clark-type YSI Standard Oxygen Probe was fitted with a fresh Teflon FEP membrane and used to determine dissolved oxygen content of solutions in a custom-made water-jacketed cell equipped with a stir bar. All measurements were made at 25.0 °C through use of a recirculating bath. The voltage response proportional to dissolved oxygen content was calibrated versus oxygen-saturated and oxygen-depleted Milli-Q water. In a typical experiment, 50 μL of a concentrated stock solution of dimer catalyst was injected into the Clark electrode cell into a solution of air-saturated Oxone triple salt ([KHSO$_5$] = 10-100 mM) in Milli-Q water. The stock solution of dimer in Milli-Q water was prepared such that injection into the sacrificial oxidant solution ensured the desired final catalyst concentration (10-50 μM). Oxygen evolved was monitored via a homebuilt LabVIEW program, and initial rates were determined by a linear least-squares fit of the data between 60 and 240 seconds.

EPR:
Differential EPR spectra were measured on a Bruker EXELSYS E500 spectrometer utilizing a super-high Q resonator and an Oxford ESR-900 helium-flow cryostat at 8.0-8.1 K. Instrument parameters included microwave frequency: 9.37 GHz; microwave power: 0.1 mW; modulation frequency: 100 kHz; modulation amplitude: 19.49 G; conversion time 20.48 ms; time constant: 40.96 ms. To prepare samples, 100 μL of a degassed solution of **2** at 0.6 mM in 0.1 M NaTFA in MeCN was frozen at the bottom of an EPR tube. This salt solution was found to improve glassing and prevent aggregation. 50 μL of degassed

9

0.1 M NaTFA in MeCN was then layered on top and frozen. Finally, a degassed solution of 6.0 mM Ph$_4$PHSO$_5$ in the NaTFA/MeCN mixture was layered on top and frozen. The spectra of frozen samples were then measured. Subsequently, samples were thawed, mixed in-tube for 30 s, refrozen, and the spectra remeasured. Three such thaw-freeze-measure cycles were performed.

Electrochemistry:

Electrochemical measurements were made with a Pine Wavenow potentiostat. A glassy carbon electrode was used as a working electrode, with a Pt wire counter electrode and an Ag/AgCl (sat. KCl) reference electrode for aqueous measurements or a Ag wire as a pseudoreference electrode. Aqueous measurements were taken in 0.1 M acetate buffer at pH = 4.47, and nonaqueous measurements were made in 0.1 M TBAPF$_6$ in MeCN. To convert measurements to a NHE reference, 0.199 V were added to all potentials from measurements made in aqueous conditions, and those made in nonaqueous conditions were referenced against Fc/Fc$^+$ and converted to NHE, taking the Fc/Fc$^+$ couple to be 630 mV vs. NHE.[49] Cyclic voltammetric measurements were made at 100 mV/s scan rates unless otherwise noted. Differential pulse voltammetric measurements were made with the following parameters including potential window: 0 - 1.2 V; pulse height: 50 mV; pulse width 10 ms; pulse period: 100 ms; pulse increment: 10 mV; sampling pre-pulse width: 3 ms; sampling post-width: 3 ms.

Spectroelectrochemistry:

Spectroelectrochemical (SEC) experiments were performed using a Pt-coated honeycomb electrode that contains both working and counter electrode capabilities and mounts into a thin-layer quartz cuvette. A separate saturated aqueous Ag/AgCl reference electrode or AgCl-coated silver wire pseudoreference electrode was utilized as appropriate. The measurements made using the former reference electrode were converted to NHE reference by adding 0.199 V, and the latter was referenced against an internal Fc/Fc$^+$ standard to convert to NHE. Samples were prepared at 2.5 mM unless otherwise noted in 0.1 M acetate buffer (pH = 4.47), 0.1 M K$_2$SO$_4$ (pH adjusted to 4.47 with H$_2$SO$_4$) or 0.1 M Bu$_4$NPF$_6$ in spectrophotometry-grade MeCN. Using a CH Instruments Model 1200B potentiostat, various potentials were applied for 15 minutes each. Current was monitored via chronoamperometry and was shown to decay towards values below 1x 10^{-7} mA in the latter half of each run, indicating equilibrium was reached at each potential before stepping to the next potential. Absorption spectra were recorded from 300-1000 nm using a Cary 50 spectrophotometer in the final few seconds of each electrolysis.

Global analysis of SEC was carried out in Origin 8.6. The spectrum found at each potential was modelled as a linear combination of the absorbance spectra of **1**, **2**, and **3,** each recorded at 2.5 mM except for **2** which was recorded at 1.25 mM to account for its dimeric structure. The coefficients for these spectra were constrained as positive values and to add up to 1. They were later expressed as percentages of total Mn.

X-ray Crystallography:

Low-temperature diffraction data (ω-scans) were collected on a Rigaku SCX Mini diffractometer coupled to a Rigaku Mercury275R CCD for structure **2** with Mo Kα radiation (λ = 0.71073 Å). Similar data were collected on a Rigaku MicroMax-007HF diffractometer coupled to a Saturn994+ CCD detector with Cu Kα (λ = 1.54178 Å) for the structures **3** of **4**. The diffraction images were processed and scaled using Crysalis Pro software for **2** and Rigaku Oxford Diffraction software for **3** and **4**. The structures were solved with SHELXT and were refined against F^2 on all data by full-matrix least squares with SHELXL. All non-hydrogen atoms were refined anisotropically. Unless stated otherwise, hydrogen atoms were first found in the difference map and then included in the model at geometrically calculated positions and refined using a riding model. The isotropic displacement parameters of all hydrogen atoms were fixed to 1.2 times the U value of the atoms to which they are linked (1.5 times for methyl groups). The full numbering scheme of **2** - **4** can be found in the full details of the X-ray structure determination (CIF), which are included as Supporting Information. CCDC files 1872330 (**2**), 1872331 (**3**), and 1872332 (**4**) contain the supplementary crystallographic data for this paper. These data can be obtained free of charge from The Cambridge Crystallographic Data Center via www.ccdc.cam.ac.uk/data_request/cif.

Acknowledgments

References

[1] J. P. McEvoy, G. W. Brudvig, *Chem. Rev.* **2006**, *106*, 4455-4483.
[2] D. J. Vinyard, G. M. Ananyev, C. G. Dismukes, *Annu. Rev. Biochem.* **2013**, *82*, 577–606.
[3] D. J. Vinyard, G. W. Brudvig, *Annu. Rev. Phys. Chem.* **2017**, *68*, 101-116.
[4] M. Pérez-Navarro, F. Neese, W. Lubitz, D. A. Pantazis, N. Cox, *Curr. Opin. Chem. Biol.* **2016**, 31, 113-119.
[5] M. D. Kärkäs, O. Verho, E. V Johnston, B. Åkermark, *Chem. Rev.* **2014**, *114*, 11863-12001.
[6] J. D. Blakemore, R. H. Crabtree, G. W. Brudvig, *Chem. Rev.* **2015**, *115,*12974-13005.

[7]   F. A. Armstrong, *Phil. Trans. R. Soc.* **2008**, *363*, 1263–1270.
[8]   J. Limburg, J. S. Vrettos, L. M. Liable-Sands, A. L. Rheingold, R. H. Crabtree, G. W. Brudvig. *Science,* **1999**, *283*, 1524-1527.
[9]   J. Limburg, J. S. Vrettos, H. Chen, J. C. de Paula, R. H. Crabtree, G. W. Brudvig, *J. Am. Chem. Soc.* **2001**, *123*, 423–430.
[10]   S. Khan, K. R. Yang, M. Z. Ertem, V. S. Batista, G. W. Brudvig, *ACS Catal.* **2015**, 7104–7113.
[11]   S. Mukhopadhyay, S. K. Mandal, S. Bhaduri, W. H. Armstrong, *Chem. Rev.* **2004**, *104*, 3981–4026.
[12]   R. H. Holm, P. Kennepohl, E. I. Solomon, *Chem Rev.***1996**, *96*, 2239-2314**.**
[13]   E. A. Karlsson, B. Lee, E. V Johnston, M. D. Kärkäs, J. Sun, Ö. Hansson, J. Bäckvall, **2011**, *5*, 11715–11718.
[14]   R. Liao, M. D. Ka, B. Lee, B. Åkermark, P. E. M. Siegbahn, *Inorg. Chem.* **2015**, *54*, 342.
[15]   A. K. Poulsen, A. Rompel, C. J. McKenzie, *Angew. Chem. Int. Ed.* **2005**, *117*, 7076–7080.
[16]   E. Y. Tsui, R. Tran, J. Yano, T. Agapie, *Nat. Chem.* **2013**,*5*, 293-299.
[17]   E. Y. Tsui, J. S. Kanady, T. Agapie, *Inorg. Chem.* **2013**, *52*, 13833-13848.
[18]   J. S. Kanady; E. Y. Tsui; M. W. Day; T. Agapie, *Science* **2011**, *333*, 733–736.
[19]   K. J. Young, M. K. Takase, G. W. Brudvig, *Inorg. Chem.* **2013**, *52*, 7615–7622.
[20]   W. A. A. Arafa, M. D. Kärkäs, B. L. Lee, T. Åkermark, R. Z. Liao, H. M. Berends, J. Messinger, P. E. M. Siegbahn, B. Åkermark, *Phys. Chem. Chem. Phys.* **2014**, *16*, 11950–11964.
[21]   R. Zong, R. P. Thummel, *J. Am. Chem. Soc.* **2005**, *127*, 12802-12803.
[22]   C. T. Carver, B. D. Matson, J. M. Mayer, *J. Am. Chem. Soc.* **2012**, *134*, 5444–5447.
[23]   R. M. Bullock, A. M. Appel, M. L. Helm, *Chem. Commun.* **2014**, *50*, 3125–3143.
[24]   D. L. Jenson, B. A. Barry, *J. Am. Chem. Soc.* **2009**, *131*, 10567–10573.
[25]   L. Vogt, D. J. Vinyard, S. Khan, G. W. Brudvig, *Curr. Opin. Chem. Biol.* **2015**, *25*, 152–158.
[26]   Y. Naruta, M. Sasayama, T. Sasaki, *Angew. Chem. Int. Ed.* **1994**, *33*, 1839–1841.
[27]   S, Kal, L. Ayensu-Mensah, P. H. Dinolfo, *Inorg. Chim. Acta.* **2014**, *423,* 201-206.
[28]   W. Lee, S. B. Muñoz III, D. A. Dickie, J. M. Smith. *Angew. Chem. Int. Ed.* **2014**, *53*, 9856-9859.
[29]   G. Maayan, N. Gluz, G. Christou, *Nat. Catal.* **2018**, *1,* 48-54.
[30]   G. W. Brudvig, *Nat. Catal.* **2018**, *1*, 10–11.
[31]   S. B. Sinha, D. Y. Shopov, L. S. Sharninghausen, D. J. Vinyard, B. Q. Mercado, G. W. Brudvig, R. H. Crabtree, *J. Am. Chem. Soc.* **2015**, *137*, 15692–15695.
[32]   S. B. Sinha, D. Y. Shopov, L. S. Sharninghausen, D. J. Vinyard, B. Q. Mercado, G. W. Brudvig, R. H. Crabtree, *J. Am. Chem. Soc.* **2015**, *137*, 15692–15695.
[33]   D. Y. Shopov, B. Rudshteyn, V. S. Batista, R. H. Crabtree, G. W. Brudvig, *J. Am. Chem. Soc.* **2015**, *137*, 7243-7250.
[34]   D. Y. Shopov, B. Rudshteyn, J. Campos, D. Vinyard, V. S. Batista, G. W. Brudvig, R. H. Crabtree, *Chem. Sci.* **2017**, *8,* 1642-1652.
[35]   D. L. Huang, R. Beltrán-Suito, J. M. Thomsen, S. M. Hashmi, K. L. Materna, S. W. Sheehan, B. Q. Mercado, G. W. Brudvig, R. H. Crabtree, *Inorg. Chem.* **2016**, *55*, 2427–2435.
[36]   J. M. Thomsen, S. W. Sheehan, S. M. Hashmi, J. Campos, U. Hintermair, R. H. Crabtree, G. W. Brudvig, *J. Am. Chem. Soc.* **2014**, *136*, 13826–13834.
[37]   J. Graeupner, U. Hintermair, D. L. Huang, J. M. Thomsen, M. Takase, *Organomet.* **2013**, *32*, 5384-5390.
[38]   K. J. Fisher, K. L. Materna, B. Q. Mercado, R. H. Crabtree, G. W. Brudvig, *ACS Catal.* **2017**, *7*, 3384–3387.
[39]   T. K. Michaelos, H. M. C. Lant, L. S. Sharninghausen, S. M. Craig, F. S. Menges, B. Q. Mercado, G. W. Brudvig, R. H. Crabtree, *Chempluschem* **2016**, *81*, 1129–1132.
[40]   A. J. Wu, J. E. Penner-Hahn, V. L. Pecoraro, *Chem. Rev.* **2004**, *104*, 903–938.
[41]   J. L. Fillol, Z. Codolà, I. Garcia-Bosch, L. Gómez, J. J. Pla, M. Costas, *Nat. Chem.* **2011**, *3*, 807-813.
[42]   D. R. Gamelin, M. Kirk, T. L. Stemmler, S Pal, W. H. Armstrong, J. E. Penner-Hahn, E. I. Solomon, *J. Am. Chem. Soc.* **1994**, *116*, 2392–2399.
[43]   S. Cooper, C. Dismukes, M. Klein, C. Melvin, *J. Am. Chem. Soc.* **1978**, *100*, 7248–7252.
[44]   M. L. Olmstead, R. G. Hamilton, R. S. Nicholson, *Anal. Chem.* **1969**, *41*, 260–267.
[45]   S. Romain, C. Duboc, M. Retegan, J. C. Leprêtre, A. G. Blackman, A. Deronzier, M. N. Collomb, *Inorg. Chim. Acta* **2011**, *374*, 187–196.
[46]   C. Baffert, S. Romain, A. Richardot, J.-C. Leprêtre, B. Lefebvre, A. Deronzier, M.-N. Collomb, *J. Am. Chem. Soc.* **2005**, *127*, 13694-13704.
[47]   H. Y. Chen; J. W. Faller; R. H. Crabtree; G. W. Brudvig, *J. Am. Chem. Soc.* **2004**, *126*, 7345–7349.
[48]   H. H. Thorp, R. H. Crabtree, G. W. Brudvig, *J. Am. Chem. Soc.* **1989**, *111*, 9249–9250.
[49]   V. V Pavlishchuk, A. W. Addison, *Inorg. Chim. Acta* **2000**, *298*, 97–102.

Entry for the Table of Contents

FULL PAPER

The complex [Mn(bipyalk)(H$_2$O)(μ-O)]$_2$(OTf)$_2$ catalyzes oxygen evolution when driven by the sacrificial oxidant KHSO$_5$ in water. A related series of the type [Mn^n(bipyalkH$_x$)(bipyalkH$_y$)](PF$_6$)$_2$, where the dication features Mn(II), (III), or (IV) oxidation states and corresponding
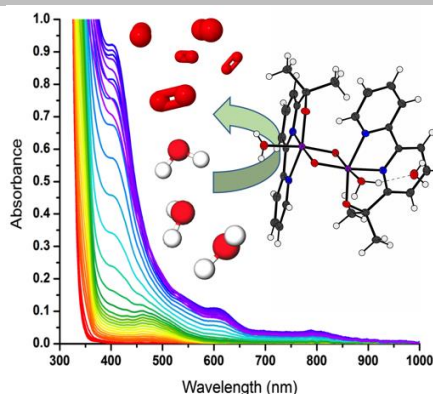
Oxygen Evolution Catalysis*
Hannah M.C. Lant[‡], Thoe K. Michaelos[a][‡], Liam S. Sharninghausen[b]; Brandon Q. Mercado; Gary W. Brudvig*; Robert H. Crabtree*

Page No. – Page No.

N,N,O Pincer Ligand with a Deprotonatable Site that Promotes Redox-Leveling, High Mn Oxidation States, and a Mn$_2$O$_2$ Dimer

protonation states, underscores
the importance of proton loss
at the alcohol/alkoxide moiety
during oxidation.

**Competent for Catalytic
Oxygen Evolution**